ACS APPLIED NANO MATERIALS
Cite This: ACS Appl. Nano Mater. 2019, 2, 1412−1420
Article
www.acsanm.org

Plasmonic Au Nanoparticles on 2D MoS_2/Graphene van der Waals Heterostructures for High-Sensitivity Surface-Enhanced Raman Spectroscopy

Mohammed Alamri,*,† Ridwan Sakidja,‡ Ryan Goul,† Samar Ghopry,† and Judy Z. Wu*,†

†Department of Physics and Astronomy, University of Kansas, Lawrence, Kansas 66045, United States
‡Department of Physics, Astronomy and Materials Science, Missouri State University, Springfield, Missouri 65897, United States

Supporting Information

ABSTRACT: A novel substrate consisting of a 2D MoS_2/graphene van der Waals (vdW) heterostructure decorated with Au nanoparticles (AuNPs) was developed for surface-enhanced Raman spectroscopy (SERS). A transfer-free chemical vapor deposition process was employed for layer-by-layer fabrication of graphene, followed with MoS_2 directly on wafers of SiO_2/Si without any metal catalyst. AuNPs were deposited on the MoS_2/graphene via *in situ* electron-beam evaporation of Au at an elevated temperature in the range of 300−350 °C under high vacuum. Rhodamine 6G (R6G) was used as an SERS probe molecule with a SERS sensitivity of 5×10^{-8} M using a nonresonance 633 nm laser, which is an order of magnitude higher than that reported on the AuNPs/graphene substrate using the same excitation. A higher SERS sensitivity of 5×10^{-10} M was obtained using resonance 532 nm laser excitation. The observed SERS sensitivity enhancement can be attributed to the combination of the electromagnetic mechanism of the plasmonic AuNPs and the chemical mechanism of the AuNPs/MoS_2/graphene vdW heterostructure via enhanced interface dipole−dipole interaction as compared to graphene or MoS_2 only as suggested by a density functional theory calculation. Therefore, this AuNPs/MoS_2/graphene vdW heterostructure is advantageous to practical applications in optoelectronics and biosensing.

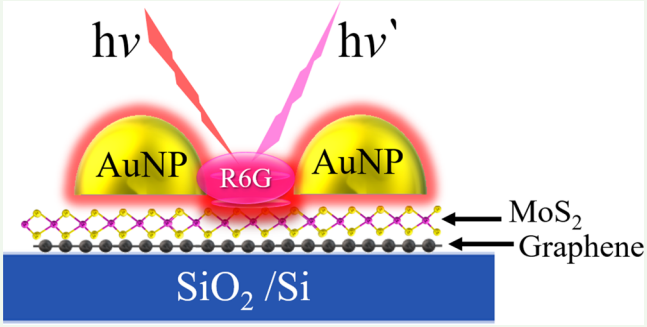

KEYWORDS: *MoS_2/graphene heterostructure, plasmonic Au nanoparticles, surface-enhanced Raman scattering, biosensing, optoelectronics*

1. INTRODUCTION

Surface-enhanced Raman spectroscopy (SERS) has been studied intensively in recent years for high-sensitivity detection of analytes such as biomolecules. SERS substrates rely on two mechanisms to enhance Raman scattering and therefore SERS sensitivity:[1−5] an electromagnetic mechanism (EM) based on an evanescent electromagnetic field created by the excitation of localized surface plasmons in the metal nanostructures, such as Au nanoparticles (AuNPs) on the substrate surface, and a chemical mechanism (CM) that originated from charge transfer through the bonding between the analyte and the substrate surface. The EM can enhance Raman scattering by orders of magnitude since the Raman signal is proportional to the squared induced dipole moment, which is proportional to a product of the polarizability and incident electromagnetic field strength. Specifically, the Raman scattering intensity scales with local electric field strength approximately $\propto E^4$.[6] Therefore, the enhanced E in the evanescent field by the plasmonic metal nanostructures is essential to the EM effect. The CM contribution is dictated by the interface electronic structures between the analyte and substrate and can be efficient by making the highest occupied molecular orbital (HOMO) to the lowest unoccupied molecular orbital (LUMO) transition more easily attainable with intermediate energy states formed through bonding to the SERS substrate. Previous work has found the EM enhancement factor of up to 10^8 be dominant over the CM's best enhancement factor which is $\sim 10^2$.[4]

Various kinds of SERS substrates based on 2D materials in combination with plasmonic metal nanostructures have been reported recently with enhanced sensitivity for biomolecule detection. Ling et al. investigated graphene SERS enhancement using probe molecules such as Rhodamine 6G (R6G) and crystal violet (CV). The observed SERS enhancement factors of 2−17 depending on the vibrational mode symmetry of the molecules on graphene, as compared to that on the SiO_2/Si substrate, are attributed to the CM effect through enhanced charge transfer between graphene and molecules. They further revealed the dependence of SERS enhancement on the number of graphene layers as the intensities of the Raman signals of the CV molecules decrease with the increasing layer number of

Received: December 20, 2018
Accepted: February 11, 2019
Published: February 11, 2019

DOI: 10.1021/acsanm.8b02308
ACS Appl. Nano Mater. 2019, 2, 1412−1420

graphene.[7] Similarly, Sun et al. reported the dependence of the Raman enhancement on the layer number of MoS_2.[8] Specifically, the Raman enhancement of monolayer MoS_2 is comparable to but slightly higher than that on MoS_2 of 2 or 3 layers. This means the SERS sensitivity is not expected to vary dramatically on MoS_2 with the layer number in the range of 1−3. However, the enhancement of 1−3 layers of MoS_2 is much higher than the bulk or multilayer MoS_2. This trend could be attributed to the reduction of the bandgap with increasing thickness of MoS_2 as a consequence of the conduction band decrease while the remaining part of the band structure remains essentially unaltered with increasing thickness. Lee et al. reported the CM enhancement of Raman signatures of R6G dip-coated onto single-layer 2D material including graphene, WSe_2, and MoS_2 substrates that were mechanically exfoliated from bulk crystals. The Raman enhancement effects of these three different substrates were observed and attributed to charge transfer and dipole−dipole interactions.[9] The Raman enhancement factors of R6G on MoS_2 and WSe_2 were about 0.5 and 1.7−2, respectively, relative to the enhancement of R6G on graphene. They fabricated R6G/graphene and R6G/MoS_2 hybrid phototransistors to study their electrical properties and observed that the Raman CM factors were correlated to the amount of the transferred charges between R6G and the 2D materials. likewise, other 2D materials such as black phosphorus (BP), rhenium disulfide (ReS_2),[10] and tin diselenide ($SnSe_2$)[11,12] have been used as SERS substrates. Lu et al. developed a hybrid AuNP/graphene SERS substrate that combines the benefits of CM enhancement from graphene with the EM enhancement of the AuNPs.[13] Using R6G probe molecules, we obtained the SERS sensitivity up to 8×10^{-7} M using a nonresonance 633 nm excitation laser.[14] In fact, a higher SERS sensitivity up to 10^{-11} M can be obtained using a resonance excitation of 532 nm for R6G probe molecules using AuNP arrays covered by a single-layer graphene.[15] More recently, Chen et al. reported a SERS substrate consisting of a few layers of MoS_2 grown on AgNPs of an average dimension of 58 nm using the thermal decomposition method. Using R6G probe molecules, they compared the SERS sensitivity of this hybrid substrate to its counterpart without the MoS_2 layer and concluded that the higher sensitivity of 10^{-9} M using 532 nm laser excitation in the former as compared to 10^{-8} M in the latter may be attributed to the combination of the CM and EM enhancements that arise from MoS_2 and AgNPs, respectively.[2]

In this work, we explore AuNPs decorated 2D MoS_2/graphene van der Waals (vdW) heterostructures for further enhancement of the SERS sensitivity. 2D vdW heterostructures present a unique platform to design SERS substrates of high CM enhancement through interface interaction of different 2D materials. In a recent theoretical work conducted by Xu et al.[16] the bonding mechanisms at the interface between graphene and MoS_2 2D layer were evaluated, which suggests that the vdW interaction can enable enhanced charge transfer and optical adsorption. Theoretically, we show further enhanced interfacial dipole−dipole interaction through AuNPs decoration on 2D MoS_2/graphene vdW heterostructures using the density functional theory (DFT) simulations. Experimentally, we illustrate a SERS sensitivity up to 5×10^{-8} M for R6G probe molecules using the AuNPs/MoS_2/graphene 2D vdW heterostructure substrate, which is an order of magnitude improvement over that on the AuNPs/graphene[14] and AuNPs/MoS_2 counterparts. The R6G sensitivity of 5×10^{-10} M was obtained on the AuNPs/MoS_2/graphene 2D vdW heterostructure substrate using resonant excitation of 532 nm, which is 1 order of magnitude higher than that reported on the AgNPs/MoS_2 substrate.[2] In the following, we report our results.

2. SIMULATION AND EXPERIMENTAL SECTION

The electronic structure of the AuNPs/MoS_2/graphene 2D vdW heterostructure was calculated using the DFT method[17] as implemented in the Vienna *ab initio* simulation package (VASP).[18,19] Specifically, these heterostructures consist of a combination of a continuous 2D layer of MoS_2 and multilayers of Au of different thicknesses. This structure was chosen to probe the interface between an AuNP of 10 nm or larger in dimensions positioned on top of a 2D MoS_2 sheet. Considering the lateral dimensions of the Au NP and the 2D MoS_2 sheet are both large, the edge effect will be negligible on the bonding mechanism at the interface, and thus a continuous layer represents a good approximation. The number of Au (111) layers was varied from $n = 1$ (monolayer) up to $n = 6$ to elucidate the effect of the Au thickness on the interface coupling.

The MoS_2/graphene 2D vdW heterostructure samples were fabricated in a layer-by-layer, transfer-free process on commercial SiO_2/Si substrates.[20] First, the transfer-free graphene was synthesized directly on SiO_2/Si substrates in a quartz tube reactor (25 mm in diameter) inside a horizontal chemical vapor deposition (CVD) furnace as reported in our previous work.[21] In a typical procedure, a clean SiO_2/Si substrate was placed at the center of the quartz tubular reactor. H_2 (120 sccm) was introduced in the reactor while it was heated to the desired temperature of 1065 °C. CH_4 (30 sccm) was then fed into the reactor to initiate graphene growth. The growth time was maintained for 3 h. After the growth of graphene, the furnace was cooled to room temperature under the protection of H_2. For synthesis of MoS_2 monolayer on the graphene/SiO_2/Si substrate, the $(NH_4)_2MoS_4$ powder was dissolved in 10 mL of *N*,*N*dimethylformamide (DMF) to make a precursor solution with a concentration of 0.1 wt %. After sonication of the precursor solution for 20 min the graphene/SiO_2/Si substrate was immersed into the $(NH_4)_2MoS_4$ precursor solution, followed by a short interval of 1 min on the spin-coater at 3000 rpm.[20] Afterward, the substrate was placed in a quartz tube CVD furnace and heated to 450 °C under a 40 sccm flow of Ar and a 10 sccm of H_2 in the presence of the sulfur vapor. The pressure in the CVD system was maintained at 50 mTorr for 1 h for MoS_2 growth. It should be noted that the direct growth of graphene on SiO_2/Si substrates can eliminate the cumbersome graphene transfer process, and it produces graphene with no contaminations that may have left after using PMMA and other chemicals during the graphene transfer process. The annealing of $(NH_4)_2MoS_4$ layer under low temperatures in the range 450−500 °C further cleans the interface of MoS_2/graphene. The interface of the transfer-free MoS_2/graphene heterostructure is cleaner than that of the similar heterostructure on transferred graphene. To decorate AuNPs on the MoS_2/graphene heterostructures, electron-beam evaporation was employed to coat 12 nm thick (nominal thickness) Au in a high vacuum of 10^{-6} Torr at 300 °C. AuNPs therefore formed *in situ* on MoS_2/graphene heterostructures as schematically illustrated in Figure 1, and this method provides additional advantages of a clean interface with the underneath layer.[13,14,22] Scanning electron microscopy (SEM, LEO 1550) was used for morphological characterization of the AuNPs. A R6G solution of the concentration 5×10^{-5} M was prepared by adding solid phase R6G (Sigma Life Science) to deionized (DI) water. The concentration of 5×10^{-5} M was further diluted for lower concentrations by mixing with DI water to obtain the desired concentration of the R6G. For Raman study, a single droplet (~10 μL) of selected concentrations of R6G solution was casted on the SERS substrate, followed with baking on a hot plate at 70 °C for 1 h before Raman characterization. Raman spectra were collected using a Witec Alpha300 confocal micro-Raman microscope. The nonresonant excitation (633 nm) and resonant excitation (532 nm) lasers were both used in Raman measurement. A Horiba iHR550

DOI: 10.1021/acsanm.8b02308
ACS Appl. Nano Mater. 2019, 2, 1412−1420

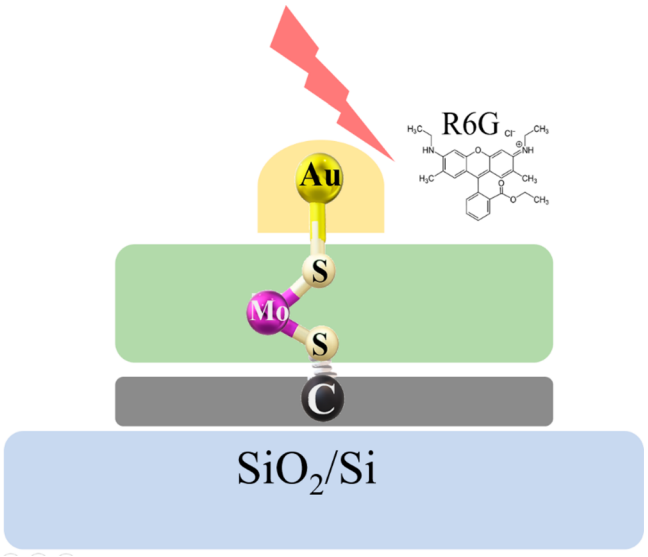

Figure 1. Schematic diagram illustrating the AuNPs/MoS_2/graphene system.

spectrometer was used for optical transmittance measurements. The integration time for each collected Raman spectrum was 3 s, and typically 4−5 spectra were taken to reduce the noise and enhance the signal-to-noise ratio.

3. RESULTS AND DISCUSSION

It should be mentioned that while there have been theoretical studies to examine the interaction between MoS_2 2D layer and Au adatom or Au (111) surface, a weak hybridization and charge transfer were concluded[23,24] at the interface, consequently resulting in a fairly large interlayer distance of 3.405 Å, as theoretically calculated,[23] and low adhesion energy (0.307−0.354 eV per surface sulfur atom).[23] However, little is known so far on the electronic structure of the interface between MoS_2 2D layer with *stacks of free-standing* Au (111) multilayers which more aptly represent the hybrid heterostructures of the AuNPs/MoS_2/graphene in this work. Intriguingly, we have found the layer thickness of the Au has a remarkable effect on the interatomic distance of the stack, which in turn affects the charge transfer mechanism of the AuNPs/MoS_2/graphene vdW heterostructures.

Figure 2 shows the side view of the Au/MoS_2 heterostructures of 1, 3, 5, and 6 monolayers of Au after the relaxation process in DFT simulation. The change in the vertical interatomic distance at the Au/MoS_2 interface can be clearly seen with varying Au layer number. While there is an apparent gradual increase with an increasing number of the Au layer at larger Au layer numbers, there is a surprisingly large initial drop (about 20%) going from an Au monolayer (1L) to two layers (2L). For 1L, we did obtain a slightly smaller interatomic distance than that reported by the previous theoretical work on bulk Au or Au adatom. This may have resulted from the use of vdW force correction in our calculations which tends to shorten the calculated bond length relative to the generalized gradient approach (GGA)-based calculations. Nevertheless, the 3.03 Å distance arguably points to a fairly weak vdW adhesion as expected from Au on MoS_2. In contrast, the remaining hybrid Au/MoS_2 heterostructures show remarkably strong bonding as hinted by the reduced interatomic distances of 2.42 Å (2L), 2.54 Å (3L), 2.57 Å (5L), and 2.59 Å (6L), which are approximately a constant (variation of only 7%) in the Au layer number range of n = 2−6. We further investigated the effect of the interactomic distance in the presence of 2 layers (2L) of MoS_2 to better resemble the experimental work. Here, for a sampling, we repeated the DFT calculations for the case of 2L of Au and 2L of MoS_2. We also tested the case when graphene is in presence underneath the 2L MoS_2. The interatomic distance remains the almost the same as shown in Figures 2b,c. This is presumably because of the relatively large distance between the Au−S position and the weak vdW interface between graphene and MoS_2. The addition of Au NPs on the multilayer MoS2 can enhance

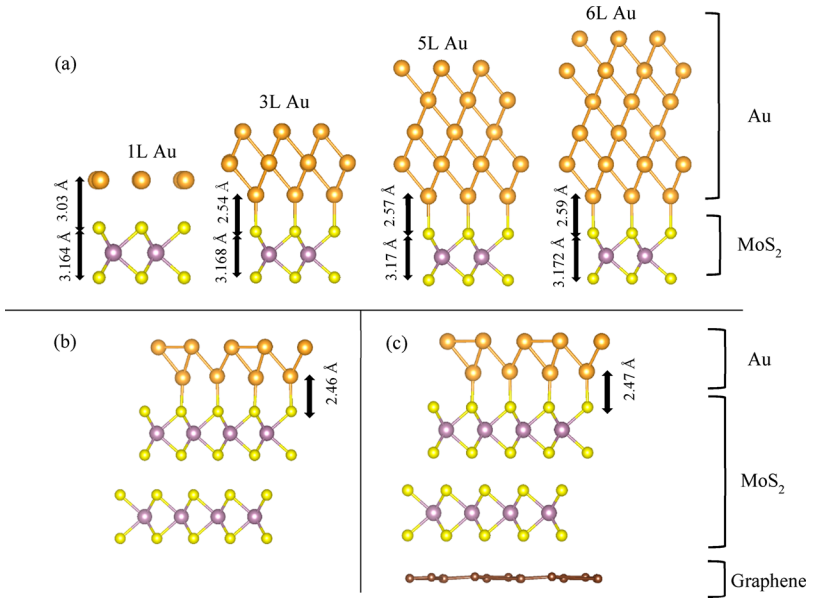

Figure 2. (a) Atomic layer stacks of Au/MoS_2 hybrid heterostructures with different numbers of Au layers of 1L, 3L, 5L, and 6L on monolayer MoS_2. The interface distance between the two materials is also illustrated. The atomic layer stacks of 2L Au/2L MoS_2 hybrid heterostructures (b) without graphene layer and (c) with graphene layer.

DOI: 10.1021/acsanm.8b02308
ACS Appl. Nano Mater. 2019, 2, 1412−1420

dipole−dipole interactions at their interface, which is known to help increase SERS assuming the impact of graphene will be similar for these samples. The agreement between the simulation and experimental observation obtained in this work is therefore interesting to the design of high-sensitivity SERS substrates based on the heterostructures of plasmonic metal nanostructures/MoS_2/graphene.

Baia et al. experimentally investigated the dependence of the R6G peak intensities on the size of the Ag NPs. Ag films with nominal thicknesses of 1, 2, 3, 4, 5, and 6 nm were used to obtain the Ag NPs with different diameters. The EM enhancement increases with increasing size of Ag NPs. However, the EM enhancement of substrates with Ag nominal thickness of 1 and 2 nm (Ag NP diameter in the range of 8−20 nm) was much weaker than that with larger thicknesses in the range of 3−6 nm (Ag NP diameter in the range of 30−55 nm). Furthermore, they found that the EM enhancement decreases with increasing the gap between Ag NPs.[25]

Figure 3 shows the 3D plots of the electron localization function (ELF) in the same hybrids of Au/MoS_2 hetero-

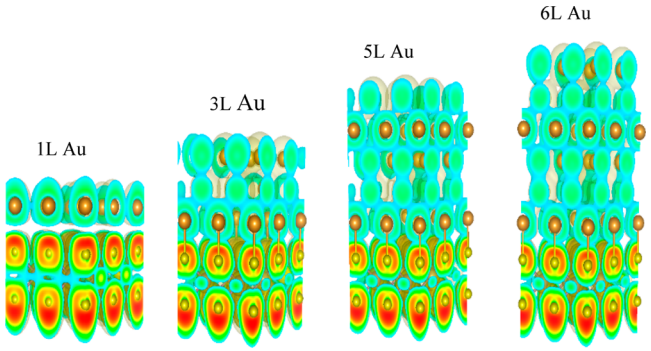

Figure 3. 3D ELF plots of the same hybrid AuNP/MoS_2 heterostructures shown in Figure 2.

structures shown in Figure 2 using the same contour range of 0.1−0.75. It should be noted that the ELF has a normalized scale of 0−1. The higher values (more red) are indicative of more localized electrons. The ELF plots from Figure 3 show a consistent picture in that there is limited electron delocalization placed at the interface when only a monolayer of Au is present. The level of electron delocalization in the presence of thicker Au layers (2L or higher L's) is remarkably higher than that in the monolayer Au case and remains relatively the same up to 6 layers, which is consistent with the minimal change in the bond length at the interface of n = 2−6. In addition, an asymmetry in the ELF (red area) surrounding the top sulfur atoms tilted toward the interface for a monolayer Au, while at larger Au layer thicknesses, a clear "C-shape" red contour structure connecting S to Mo can be seen, indicating that the strengthened Au−S bonding may have partly resulted from the weakening of the Mo−S internal bond with the 2D structures when the Au layers get thicker. This is also reflected in the slight increase, on average, of the thickness of the MoS_2 2D layer marked by the interatomic distance between the two S layers (see Figure 2).

Figure 4 shows the difference in the density of states (DOS) for the case of the Au monolayer versus the Au double layers. Specifically, we compare the partial DOS of the d-orbitals from the Au atom at the interface. By comparison of Figures 4a and 4b, it has been found that the d-band's contribution from d_{z^2} (green line) which would orientate spatially toward the S atoms is much broader, extending to 8 eV below the Fermi level in Au 2L, in contrast to 5 eV below the Fermi level for the Au 1L. The same, to a lesser extent, can be observed with the d_{xz} and d_{yz} orbitals. This DOS broadening of the z-containing d bands can be understood from the fact that the d orbitals are overlapped with the p orbitals from the terminating S atoms. As shown in Figure 4c for Au 1L, the local DOS contribution from S atoms (which also overlaps with Mo atoms as expected) spans up to the same extended energy range. This again confirms the enhanced bonding beyond the normal vdW

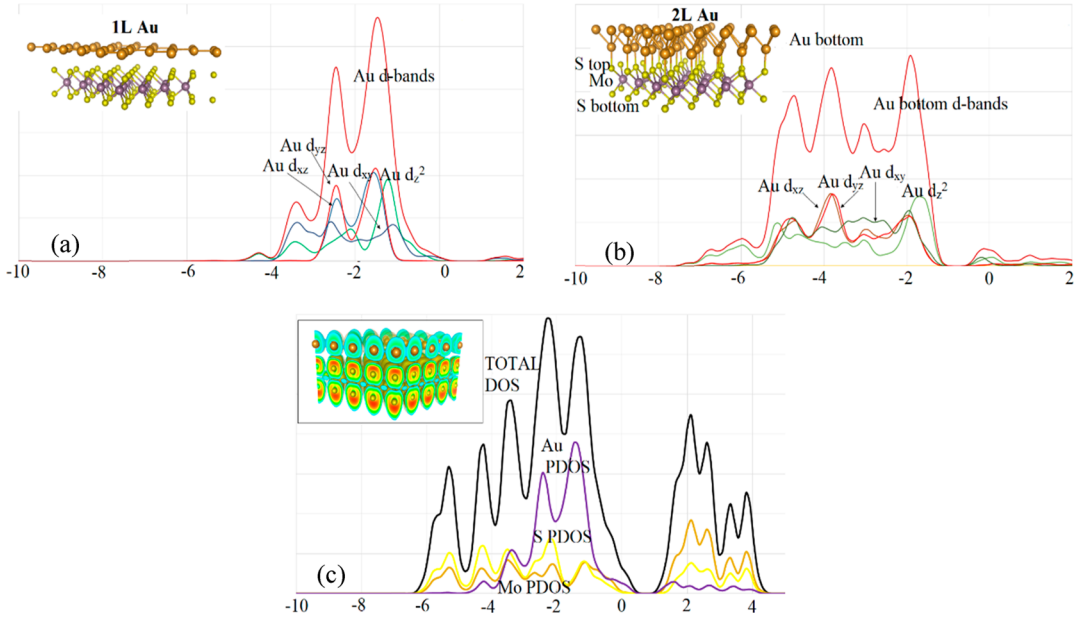

Figure 4. Comparison of the local DOS of Au atoms for (a) 1L and (b) 2L from the different types of occupied d orbitals; namely, d_{xy}, d_{xz}, d_{yz}, and d_{z^2} are minimally occupied. The total DOS and each atom-specific contribution for 1L are also shown in (c). The zero point for the energy range is the Fermi energy E_{Fermi}.

DOI: 10.1021/acsanm.8b02308
ACS Appl. Nano Mater. 2019, 2, 1412−1420

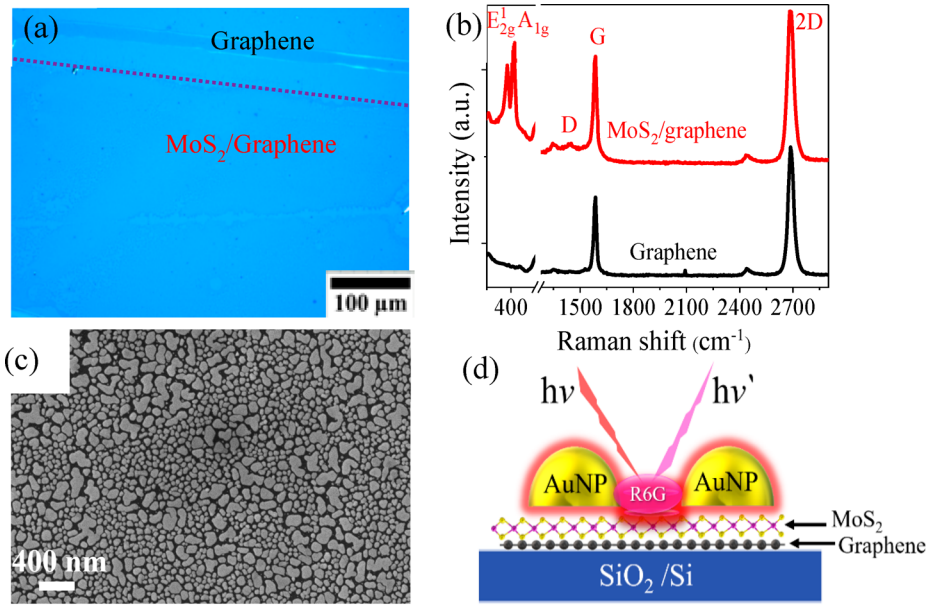

Figure 5. (a) Optical image of the MoS_2/graphene and graphene. (b) Raman spectra of MoS_2/graphene and graphene. (c) SEM of AuNPs on the MoS_2/graphene. (d) Schematic illustration of R6G on SERS substrate.

expected at the Au/MoS_2 interface with 2L or thicker Au. The DOS for thicker Au (3−6 layers) are almost similar, as illustrated in Figures S1−S4. For example, the d-band's contribution from d_z^2 extended to ∼8 eV for Au of thickness in the range of 2L−6L. We performed the same analysis on the overlap between the partial DOS's contributed by S and Au atoms to the total DOS. Figure S5 shows the results of electronic calculations for a case of 2L Au + 2L of MoS_2 as a sampling. The result is quite consistent with that of 2L Au + 1L of MoS_2. As already pointed out in the earlier part of this paper, the main effect as far as the electronic structures as concerned between 1L and 2L of a stand-alone 2D structure of MoS_2 is the change that is associated with the switch from direct (of 1.9 eV) band gap to (smaller) indirect.[26] We should note that the band gap resulting from DFT calculations here using nonhybrid potentials in general is typically underestimated, which is a known effect.[27] Our goal here is mainly to highlight the role Au layers and bonding interactions between Au and terminating S atoms from MoS_2.

Previous study has shown that as you increase the number of layers of MoS_2 2D structure, there is a reduction of the conduction band states and their minimum position in the vicinity of the Γ point (along the Γ → K direction).[26] This decrease in the conduction band minimum results in the switch to a smaller direct band gap at the K point to the indirect band gap near halfway of Γ → K. Indeed, as you further increase the number of layers, the band gap will continue (gradually) to reduce and form the reported small band gap of 1.29 eV for a bulk MoS_2. Because all of the samples being used here have relatively the same thickness, i.e., 2L or slightly thicker, a similar effect of a slightly reduced band gap (relative to that of monolayer MoS_2) will be observed for all of the samples, presumably providing relative ease for the charge transfer to take place in comparison, for example, if we were to use a single-layer MoS_2. Nevertheless, the main effect is still the increased hybridization at the top of the MoS_2 layer facilitated by the bonding between the S atoms and the multiple layers of Au.

Figure 5a displays an optical image of a representative MoS_2/graphene vdW heterostructure, which is uniform in a large area. The top part of the sample (above the dashed line) was purposely not coated with MoS_2 for convenience of the characterization. Figure 5b shows Raman spectra of graphene (above the dashed line in Figure 5a) and MoS_2/graphene vdW heterostructure (below the dashed line in Figure 5a). In both spectra, the Raman characteristic peaks at ∼1586 and 2722 nm^{-1} correspond to the G and 2D bands of graphene, respectively.[28−30] The G peak corresponds to the E_g^2 phonon at the Brillouin zone center, and the 2D peak is the second-order harmonic of the D peak that corresponds to A_{1g} breathing mode.[31] High-quality single-layer graphene is confirmed by the high ratio of the 2D and G band intensities (I_{2D}/I_G ∼ 1.7) and the negligible intensity of D the peak associated with the defects in pristine graphene and graphene after MoS_2 growth. The I_{2D}/I_G ratio of graphene has been found to be affected by the interfacial interaction of graphene with MoS_2 (or possibly other materials). For example, in a previous work by our group,[13] we have found the ratio of I_{2D}/I_G peaks decreases with increasing plasmonic Au nanoparticle dimension. The enhancement of 2D and G peaks of graphene is attributed to interface charge doping of MoS_2 from the Au, which in turn affects the charge transfer (CM effect) across the MoS_2/graphene interface. This doping affects significantly the scattering intensity via electron−electron interaction. The two characteristic peaks of MoS_2 are clearly visible in Figure 5b at 384 and 406 cm^{-1}, corresponding to the in-plane E_{1g}^2 mode and out-of-plane A_{1g} mode. The frequency difference between the two modes is ∼22 cm^{-1}, which indicates that the synthesized MoS_2 on graphene is an ultrathin layer (∼2−3 layers). The transfer-free process results in clean interfaces which is an important to charge transfer across the interfaces in the AuNPs/MoS_2/graphene vdW heterostructures. Liu et al. reported a higher performance of transfer-free MoS_2/graphene vdW heterostructure photodetector as compared to counterpart using transferred graphene.[20] The atomic force microscope (AFM) image of MoS_2 is shown in Figure S6a, revealing the thickness and the uniformity of the MoS_2 on graphene.

DOI: 10.1021/acsanm.8b02308
ACS Appl. Nano Mater. 2019, 2, 1412−1420

From the height profile, in Figure S6b, measured along the dashed line in the image, the thickness is 2.2 nm, confirming the number of layers for MoS_2 (2−3 layers). The morphology and distribution of the AuNPs on MoS_2/graphene heterostructure were characterized using SEM, as shown in Figure 5c. The AuNPs size range is 40−100 nm in diameter. Figure 5d illustrates schematically the AuNPs/MoS_2/graphene vdW heterostructure with R6G probe molecules in the SERS study with both EM enhancement from a high electromagnetic field enhanced by the plasmonic AuNPs and CM enhancement provided by the AuNPs/MoS_2/graphene vdW heterostructure. Therefore, the Raman signals of the R6G molecules at the gaps between AuNPs on the MoS_2/graphene vdW heterostructure are expected to have a significant Raman enhancement.

The optical transmission spectra of the graphene, MoS_2/graphene, and AuNPs/MoS_2/graphene samples over the wavelength range of 400−800 nm were taken to confirm the plasmonic resonance associated with the AuNPs, and the results are illustrated in Figure 6a. The spectra for the graphene

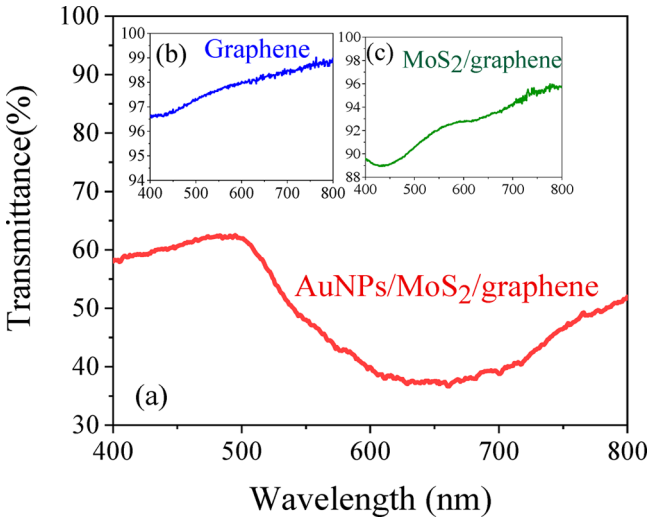

Figure 6. (a) Optical transmittance spectra of multiple materials on fused silica: (a) AuNPs/MoS_2/graphene, (b) graphene, and (c) MoS_2/graphene.

and MoS_2/graphene samples show high transparency with the minimum optical transmittance of ∼97% and 90%, respectively, in the spectral range studied. In contrast, the spectrum AuNPs/MoS_2/graphene shows a broad valley with much reduced transmission between 550 and 700 nm, indicating surface plasmonic resonance near the resonance frequencies at frequency of 650 nm due to the LSPR enhanced the light absorption in the AuNPs where the average size of AuNPs is ∼50 nm in diameter. In AuNPs/graphene with average size of 40 nm, the LSPR wavelength is ∼570 nm[14] and ∼535 nm for MoS_2/AuNPs[32] with an average size of 6 nm. However, the broad LSPR peak is not a surprise considering the large range of the AuNP dimension formed on MoS_2/graphene samples via self-assembly.[22]

In Figure 7, the Raman spectra of R6G (5×10^{-5} M) taken on different substrates are compared. A significant difference in the peak intensity of the R6G Raman signatures on different substrates is illustrated. On the single layer MoS_2 substrate (black), the R6G peaks are not visible, which is not surprising since a semiconductive MoS_2 layer is not expected to have visible CM and EM enhancement. In contrast, the R6G Raman

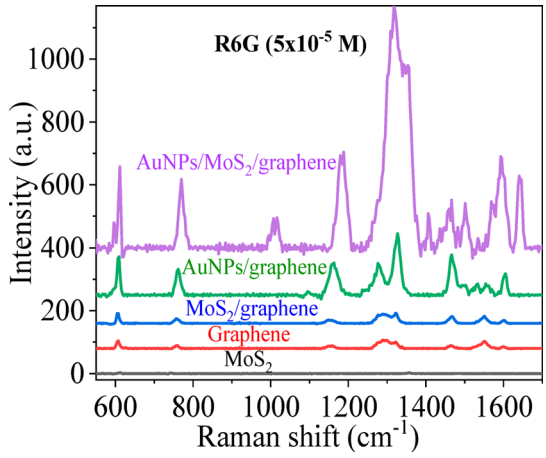

Figure 7. R6G Raman spectra of 5×10^{-5} M concentration with different substrates: AuNPs/MoS_2/graphene (purple), AuNPs/graphene (green), MoS_2/graphene (blue), graphene (red), and MoS_2 (black).

signature peaks can be clearly seen on graphene substrate (red), most probably due to the SERS enhancement via the CM mechanism.[7,9] Interestingly, further improved R6G signals can be observed on the MoS_2/graphene heterostructure substrate (blue), confirming the further enhanced CM effect predicted in theory through the vdW interaction at the MoS_2/graphene interface.[16] With decoration of the AuNPs on the MoS_2/graphene heterostructure substrate (purple), the R6G Raman signals are dramatically enhanced, which can be attributed to the combined benefits of the EM enhancement by the plasmonic AuNPs and the CM enhancement from the MoS_2/graphene vdW heterostructure. Most importantly, this R6G SERS enhancement on the AuNPs/MoS_2/graphene vdW heterostructure is much more significant than on the AuNPs/graphene (green) substrate with similar AuNPs made in the same process on graphene, indicating the interlayer coupling in the hybrid AuNPs/MoS_2/graphene heterostructure indeed plays an critical role in further enhancing the CM effect.[33,34] Therefore, the Raman signals of R6G on AuNPs/MoS_2/graphene substrate have the highest SERS effect among the five substrates tested in Figure 7 due to the combination of the EM and CM enhancements[35] arising from AuNPs/MoS_2/graphene heterostructure with the EM enhancement by AuNPs dominating the enhancement.[36,37] Additional spectral features of R6G, such as R6G peak at ∼1088 cm^{-1} in Figure 7, can be detected only at higher SERS enhancement on AuNPs/MoS_2/graphene SERS substrates. All SERS measurements were taken at a low level of the laser power (∼1 mW) to avoid any damage to the R6G molecules. Figure S7 shows the SERS measurements at different laser power to illustrate the effect of exciting laser power on Raman signals of the R6G molecules. Raman signals increase with increasing laser power (0.05−0.2 mW) and saturated (0.5−5 mW). The decrease in the R6G signals at a higher power (at 10 mW) is attributed to the damage of the molecules during the collection time of 3 s. To get reasonable measurements and avoiding molecules damage, a laser power of 1 mW was selected.

The R6G Raman spectra of different R6G concentrations on AuNPs/MoS_2/graphene are shown in Figure 8. These spectra were obtained with both a nonresonance 633 nm excitation (Figure 8a) and a resonance 532 nm (Figure 8b) laser. While a higher Raman sensitivity can be typically obtained at the

DOI: 10.1021/acsanm.8b02308
ACS Appl. Nano Mater. 2019, 2, 1412−1420

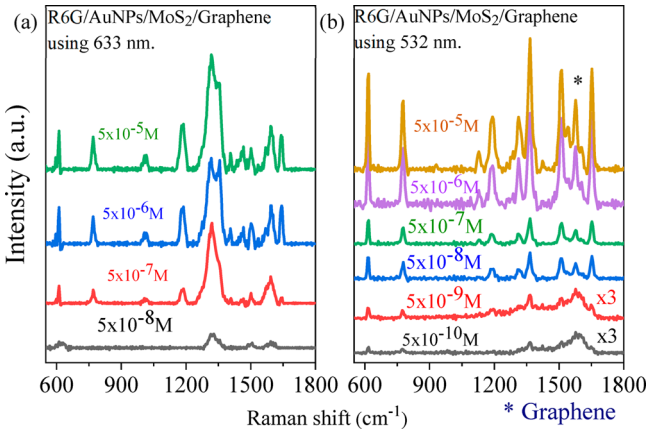

Figure 8. Raman spectra of the R6G molecules with different concentrations cast on the AuNPs/MoS_2/graphene hybrid using (a) 633 nm laser and (b) a 532 nm laser. Spectra of concentrations 5×10^{-9} and 5×10^{-10} M were multiplied by a factor of 3.

resonance of the probe molecules, the nonresonance excitation provides the practical limit of the SERS sensitivity for a large variety of the molecules that may not have compatible resonance excitations available for SERS. The characteristic Raman peaks of R6G are clearly visible with both types of excitations. Specifically, the 612 cm^{-1} peak is assigned to C−C−C ring in-plane vibration, 769 and 1088 cm^{-1} peaks to the C−H out-of-plane bend, 1184 cm^{-1} peak to C−C stretching vibrations, and the 1320 and 1502 cm^{-1} peaks to the N−H in-plane bend, while the 1361, 1502, and 1663 cm^{-1} peaks are assigned to C−C stretching.[38,39] The intensity of R6G Raman peaks decreases monotonically with the R6G concentration. The minimum detectable R6G concentration on the AuNPs/MoS_2/graphene substrate using 633 nm laser is about 5×10^{-8} M, at which not all R6G peaks are observable as shown in Figure 8a. A lower concentration of 5×10^{-9} M was also tested, but no Raman signal could be detected for R6G. It should be noted that the R6G sensitivity of 5×10^{-8} M on the AuNPs/MoS_2/graphene substrates is about an order of magnitude higher than that of the AuNPs/graphene substrates reported previously.[14] Thus, this result illustrates that inserting a MoS_2 layer between the AuNPs and graphene can improve the SERS sensitivity by enhancing the CM effect through interface electronic structure modification of the AuNPs/MoS_2/graphene vdW heterostructures. In Figure 8b, the R6G detection limit of 5×10^{-10} M is obtained using the resonant excitation wavelength of 532 nm, which is 1 order of magnitude higher than that reported on the AgNPs/MoS_2 substrate using a 532 nm laser.[2] In addition, the Raman spectra of the R6G on AuNPs/MoS_2 were collected as shown in Figure S7 with lower sensitivity of about 5×10^{-7} M (Figure S7a) and 5×10^{-9} M (Figure S7b) respectively using 633 and 532 nm lasers. The AuNPs on MoS_2/graphene heterostructure substrate shows a higher enhancement compared to AuNPs on graphene or MoS_2 only.

In should be mentioned that many interesting approaches have been reported for molecule detection[40−44] using 2D materials, and single molecule sensitivity has been reported.[42] However, Raman spectroscopy, especially in combination with SERS substrates that can be fabricated using low-cost scalable processes, provides a viable approach for high-sensitivity molecule recognition through the Raman signature of specific molecules.[45,46]

A quantitative analysis was made on three distinct peaks of the R6G at 612, 767, and 1184 cm^{-1} to investigate the relationship between the Raman intensity and the concentrations of the R6G molecules with 633 and 532 nm laser excitation. Figures 9a−c show a linear relation between the Raman peaks intensity as a function of the R6G concentrations. The Raman peaks intensity saturate as the concentration of the R6G is increased. Figures 9d−f replot the data in the Figures 9a−c on a log scale, illustrating a good linear relationship between SERS intensity and the R6G concentrations. The trends indicate that the Raman signals intensity decrease with the decreasing R6G concentration as has been reported in several studies.[47,48]

4. CONCLUSION

In conclusion, this work reports a new SERS substrate based on plasmonic AuNPs decorated 2D MoS_2/graphene vdW heterostructures made using a transfer-free layer-by-layer process, which has advantages for scale-up to large wafers as

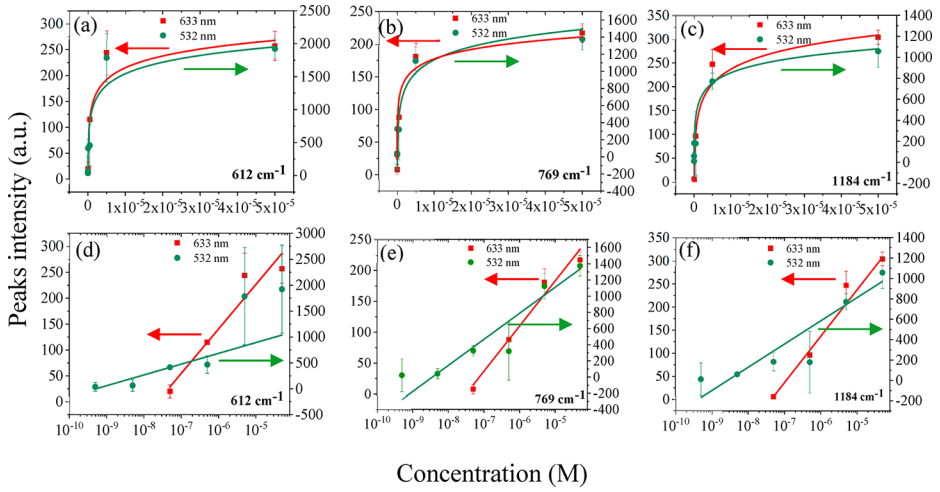

Figure 9. Intensities of the Raman peaks as a function of the R6G concentrations at (a, d) 612 cm^{-1}, (b, e) 769 cm^{-1}, and (c, f) 1184 cm^{-1} for the AuNPs/MoS_2/graphene substrates using both 633 nm laser (red) and 532 nm laser (green). Panels d, e, and f were plotted using a logarithmic scale.

DOI: 10.1021/acsanm.8b02308
ACS Appl. Nano Mater. 2019, 2, 1412−1420

well as clean interfaces for optimal charge transfer across the interfaces in the AuNPs/MoS_2/graphene vdW heterostructures. Using R6G as probe molecules, we investigated the SERS sensitivity using both nonresonant excitation of a 633 nm laser and a resonant 532 nm laser. In the former, the R6G SERS sensitivity of 5×10^{-8} M was obtained, which is an order of magnitude higher than the best reported on AuNPs/graphene substrates. This enhancement may be attributed to the enhanced dipole−dipole interaction at the Au/MoS_2 interface at large Au thickness in exceeding two monolayers as revealed in the DFT simulation. This enhanced interface interaction results in enhanced electron delocalization and hence enhanced CM contribution to SERS signatures. By use of resonance excitation of a 532 nm laser, a higher SERS sensitivity of 5×10^{-10} M was achieved for R6G on AuNPs/MoS_2/graphene substrates, which is also an order of magnitude higher than that reported on AgNPs/MoS_2 substrate using the same 532 nm excitation. This result illustrates a pathway in design high-performance SERS substrates based on 2D vdW heterostructures for optimal CM contribution to SERS, which can be combined with the plasmonic metal nanostructures, such as AuNPs in this work, for high-sensitivity SERS.

■ ASSOCIATED CONTENT

Supporting Information

The Supporting Information is available free of charge on the ACS Publications website at DOI: 10.1021/acsanm.8b02308.

Figure S1: (a) ELF and (b) DOS plots of Au 3L + MoS_2; Figure S2: (a) ELF and (b) DOS plots of Au 4L + MoS_2; Figure S3: (a) ELF and (b) DOS plots of Au 5L + MoS_2; Figure S4: (a) ELF and (b) DOS plots of Au 6L + MoS_2; Figure S5: (a) higher resolution plots of DOS for 2L Au + 2L MoS_2 and (b) DOS plots of 2L Au + 2L MoS_2 + graphene (for these DOS plots, we employed tetrahedron method with a *k*-point sampling of a 5−5−1 grid corresponding to 13 irreducible *k*-points; in both cases, the DOS near the Fermi energy level is dominated by the hybridization of p-orbitals of S and d-orbitals of Au and Mo); Figure S6: (a) an AFM image of the MoS_2 on graphene and (b) the height profile along the dashed yellow line in (a) with average thickness of ∼2.2 nm; Figure S7: Raman spectra of the R6G taken by the 633 nm laser with different laser powers (0.05−10 mW); Figure S8: Raman spectra of the R6G molecules with different concentrations cast on the AuNPs/MoS_2hybrid using (a) a 532 laser (spectra of concentrations 5×10^{-8} and 5×10^{-9} M were multiplied by a factor of 5) and (b) 633 nm laser (PDF)

■ AUTHOR INFORMATION

Corresponding Authors

*(M.A.) E-mail mohammed.alamri@ku.edu.
*(J.Z.W.) E-mail jwu@ku.edu.

ORCID

Mohammed Alamri: 0000-0002-7473-8644

Author Contributions

M.A. and J.W. designed the experiment. R.S. did the simulation. M.A. performed sample characterization. R.G. and S.G. participated in sample preparation. M.A. and J.W. led the effort in manuscript writing. All authors contributed to discussions of the results and development of the manuscript.

Notes

The authors declare no competing financial interest.

■ ACKNOWLEDGMENTS

The authors acknowledge support in part by ARO Contracts ARO-W911NF-16-1-0029 and NSF Contracts NSF-ECCS-1809293/1809284 and NSF-DMR-1508494. M.A. acknowledges the support from the Umm Al-Qura University.

■ REFERENCES

(1) Qiu, H.; Xu, S.; Chen, P.; Gao, S.; Li, Z.; Zhang, C.; Jiang, S.; Liu, M.; Li, H.; Feng, D. A Novel Surface-Enhanced Raman Spectroscopy Substrate Based on Hybrid Structure of Monolayer Graphene and Cu Nanoparticles for Adenosine Detection. *Appl. Surf. Sci.* **2015**, *332*, 614−619.

(2) Chen, P.; Qiu, H.; Xu, S.; Liu, X.; Li, Z.; Hu, L.; Li, C.; Guo, J.; Jiang, S.; Huo, Y. A Novel Surface-Enhanced Raman Spectroscopy Substrate Based on a Large Area of MoS_2 and Ag Nanoparticles Hybrid System. *Appl. Surf. Sci.* **2016**, *375*, 207−214.

(3) Geng, X.; Jiao, Y.; Han, Y.; Mukhopadhyay, A.; Yang, L.; Zhu, H. Freestanding Metallic 1t MoS_2 with Dual Ion Diffusion Paths as High Rate Anode for Sodium-Ion Batteries. *Adv. Funct. Mater.* **2017**, DOI: 10.1002/adfm.201770234.

(4) Schlücker, S. Surface-Enhanced Raman Spectroscopy: Concepts and Chemical Applications. *Angew. Chem., Int. Ed.* **2014**, *53* (19), 4756−4795.

(5) Feng, S.; dos Santos, M. C.; Carvalho, B. R.; Lv, R.; Li, Q.; Fujisawa, K.; Elías, A. L.; Lei, Y.; Perea-López, N.; Endo, M.; et al. Ultrasensitive Molecular Sensor Using N-Doped Graphene through Enhanced Raman Scattering. *Sci. Adv.* **2016**, *2* (7), e1600322.

(6) Stiles, P. L.; Dieringer, J. A.; Shah, N. C.; Van Duyne, R. P. Surface-Enhanced Raman Spectroscopy. *Annu. Rev. Anal. Chem.* **2008**, *1*, 601−626.

(7) Ling, X.; Xie, L.; Fang, Y.; Xu, H.; Zhang, H.; Kong, J.; Dresselhaus, M. S.; Zhang, J.; Liu, Z. Can Graphene Be Used as a Substrate for Raman Enhancement? *Nano Lett.* **2010**, *10* (2), 553−561.

(8) Sun, L.; Hu, H.; Zhan, D.; Yan, J.; Liu, L.; Teguh, J. S.; Yeow, E. K.; Lee, P. S.; Shen, Z. Plasma Modified Mos2 Nanoflakes for Surface Enhanced Raman Scattering. *Small* **2014**, *10* (6), 1090−1095.

(9) Lee, Y.; Kim, H.; Lee, J.; Yu, S. H.; Hwang, E.; Lee, C.; Ahn, J.-H.; Cho, J. H. Enhanced Raman Scattering of Rhodamine 6G Films on Two-Dimensional Transition Metal Dichalcogenides Correlated to Photoinduced Charge Transfer. *Chem. Mater.* **2016**, *28* (1), 180−187.

(10) Lin, J.; Liang, L.; Ling, X.; Zhang, S.; Mao, N.; Zhang, N.; Sumpter, B. G.; Meunier, V.; Tong, L.; Zhang, J. Enhanced Raman Scattering on in-Plane Anisotropic Layered Materials. *J. Am. Chem. Soc.* **2015**, *137* (49), 15511−15517.

(11) Zhang, Y.; Shi, Y.; Wu, M.; Zhang, K.; Man, B.; Liu, M. Synthesis and Surface-Enhanced Raman Scattering of Ultrathin $SnSe_2$ Nanoflakes by Chemical Vapor Deposition. *Nanomaterials* **2018**, *8* (7), 515.

(12) Liu, M.; Shi, Y.; Zhang, G.; Zhang, Y.; Wu, M.; Ren, J.; Man, B. Surface-Enhanced Raman Spectroscopy of Two-Dimensional Tin Diselenide Nanoplates. *Appl. Spectrosc.* **2018**, *72* (11), 1613−1620.

(13) Lu, R.; Konzelmann, A.; Xu, F.; Gong, Y.; Liu, J.; Liu, Q.; Xin, M.; Hui, R.; Wu, J. Z. High Sensitivity Surface Enhanced Raman Spectroscopy of R6G on in Situ Fabricated Au Nanoparticle/Graphene Plasmonic Substrates. *Carbon* **2015**, *86*, 78−85.

(14) Goul, R.; Das, S.; Liu, Q.; Xin, M.; Lu, R.; Hui, R.; Wu, J. Z. Quantitative Analysis of Surface Enhanced Raman Spectroscopy of Rhodamine 6G Using a Composite Graphene and Plasmonic Au Nanoparticle Substrate. *Carbon* **2017**, *111*, 386−392.

(15) Xu, S.; Jiang, S.; Wang, J.; Wei, J.; Yue, W.; Ma, Y. Graphene Isolated Au Nanoparticle Arrays with High Reproducibility for High-Performance Surface-Enhanced Raman Scattering. *Sens. Actuators, B* **2016**, *222*, 1175−1183.

DOI: 10.1021/acsanm.8b02308
ACS Appl. Nano Mater. 2019, 2, 1412−1420

(16) Xu, L.; Huang, W.-Q.; Hu, W.; Yang, K.; Zhou, B.-X.; Pan, A.; Huang, G.-F. Two-Dimensional MoS_2-Graphene-Based Multilayer Van Der Waals Heterostructures: Enhanced Charge Transfer and Optical Absorption, and Electric-Field Tunable Dirac Point and Band Gap. *Chem. Mater.* **2017**, *29* (13), 5504−5512.
(17) Kohn, W.; Sham, L. J. Self-Consistent Equations Including Exchange and Correlation Effects. *Phys. Rev.* **1965**, *140* (4A), A1133−A1138.
(18) Kresse, G.; Furthmüller, J. Efficiency of Ab-Initio Total Energy Calculations for Metals and Semiconductors Using a Plane-Wave Basis Set. *Comput. Mater. Sci.* **1996**, *6* (1), 15−50.
(19) Kresse, G.; Furthmüller, J. Efficient Iterative Schemes for Ab Initio Total-Energy Calculations Using a Plane-Wave Basis Set. *Phys. Rev. B: Condens. Matter Mater. Phys.* **1996**, *54* (16), 11169−11186.
(20) Liu, Q.; Cook, B.; Gong, M.; Gong, Y.; Ewing, D.; Casper, M.; Stramel, A.; Wu, J. Printable Transfer-Free and Wafer-Size MoS_2/Graphene Van Der Waals Heterostructures for High-Performance Photodetection. *ACS Appl. Mater. Interfaces* **2017**, *9* (14), 12728−12733.
(21) Liu, Q.; Gong, Y.; Wang, T.; Chan, W.-L.; Wu, J. Metal-Catalyst-Free and Controllable Growth of High-Quality Monolayer and Ab-Stacked Bilayer Graphene on Silicon Dioxide. *Carbon* **2016**, *96*, 203−211.
(22) Xu, G. W.; Liu, J. W.; Wang, Q.; Hui, R. Q.; Chen, Z. J.; Maroni, V. A.; Wu, J. Plasmonic Graphene Transparent Conductors. *Adv. Mater.* **2012**, *24* (10), OP71−OP76.
(23) Zhong, H.; Quhe, R.; Wang, Y.; Ni, Z.; Ye, M.; Song, Z.; Pan, Y.; Yang, J.; Yang, L.; Lei, M.; Shi, J.; Lu, J. Interfacial Properties of Monolayer and Bilayer MoS_2 Contacts with Metals: Beyond the Energy Band Calculations. *Sci. Rep.* **2016**, *6*, 21786.
(24) Chang, J.; Larentis, S.; Tutuc, E.; Register, L. F.; Banerjee, S. K. Atomistic Simulation of the Electronic States of Adatoms in Monolayer MoS_2. *Appl. Phys. Lett.* **2014**, *104* (14), 141603.
(25) Bai, Y.; Yan, L.; Wang, J.; Su, L.; Chen, N.; Tan, Z. Highly Reproducible and Uniform Sers Substrates Based on Ag Nanoparticles with Optimized Size and Gap. *Photonics and Nanostructures-Fundamentals and Applications* **2017**, *23*, 58−63.
(26) Ganatra, R.; Zhang, Q. Few-Layer Mos2: A Promising Layered Semiconductor. *ACS Nano* **2014**, *8* (5), 4074−4099.
(27) Crowley, J. M.; Tahir-Kheli, J.; Goddard, W. A. Resolution of the Band Gap Prediction Problem for Materials Design. *J. Phys. Chem. Lett.* **2016**, *7* (7), 1198−1203.
(28) Deokar, G.; Avila, J.; Razado-Colambo, I.; Codron, J.-L.; Boyaval, C.; Galopin, E.; Asensio, M.-C.; Vignaud, D. Towards High Quality Cvd Graphene Growth and Transfer. *Carbon* **2015**, *89*, 82−92.
(29) Barin, G. B.; Song, Y.; de Fátima Gimenez, I.; Souza Filho, A. G.; Barreto, L. S.; Kong, J. Optimized Graphene Transfer: Influence of Polymethylmethacrylate (Pmma) Layer Concentration and Baking Time on Graphene Final Performance. *Carbon* **2015**, *84*, 82−90.
(30) Marta, B.; Leordean, C.; Istvan, T.; Botiz, I.; Astilean, S. Efficient Etching-Free Transfer of High Quality, Large-Area Cvd Grown Graphene onto Polyvinyl Alcohol Films. *Appl. Surf. Sci.* **2016**, *363*, 613−618.
(31) Ferrari, A. C.; Basko, D. M. Raman Spectroscopy as a Versatile Tool for Studying the Properties of Graphene. *Nat. Nanotechnol.* **2013**, *8* (4), 235−246.
(32) Chuang, M.-K.; Yang, S.-S.; Chen, F.-C. Metal Nanoparticle-Decorated Two-Dimensional Molybdenum Sulfide for Plasmonic-Enhanced Polymer Photovoltaic Devices. *Materials* **2015**, *8* (8), 5414−5425.
(33) Tan, Y.; Ma, L.; Gao, Z.; Chen, M.; Chen, F. Two-Dimensional Heterostructure as a Platform for Surface-Enhanced Raman Scattering. *Nano Lett.* **2017**, *17* (4), 2621−2626.
(34) Chang, K.; Mei, Z.; Wang, T.; Kang, Q.; Ouyang, S.; Ye, J. MoS_2/Graphene Cocatalyst for Efficient Photocatalytic H2 Evolution under Visible Light Irradiation. *ACS Nano* **2014**, *8* (7), 7078−7087.
(35) Zhao, Y.; Pan, X.; Zhang, L.; Xu, Y.; Li, C.; Wang, J.; Ou, J.; Xiu, X.; Man, B.; Yang, C. Dense Aunp/Mos 2 Hybrid Fabrication on Fiber Membranes for Molecule Separation and Sers Detection. *RSC Adv.* **2017**, *7* (58), 36516−36524.
(36) Qiu, C.; Zhou, H.; Yang, H.; Chen, M.; Guo, Y.; Sun, L. Investigation of N-Layer Graphenes as Substrates for Raman Enhancement of Crystal Violet. *J. Phys. Chem. C* **2011**, *115* (20), 10019−10025.
(37) Park, W.-H.; Kim, Z. H. Charge Transfer Enhancement in the Sers of a Single Molecule. *Nano Lett.* **2010**, *10* (10), 4040−4048.
(38) Huh, S.; Park, J.; Kim, Y. S.; Kim, K. S.; Hong, B. H.; Nam, J.-M. Uv/Ozone-Oxidized Large-Scale Graphene Platform with Large Chemical Enhancement in Surface-Enhanced Raman Scattering. *ACS Nano* **2011**, *5* (12), 9799−9806.
(39) Hou, M.-J.; Zhang, X.; Cui, X.-Y.; Liu, C.; Li, Z.-C.; Zhang, Z.-J. Preparation of SiO_2@ Au Nanorod Array as Novel Surface Enhanced Raman Substrate for Trace Pollutants Detection. *Chin. Phys. B* **2015**, *24* (3), 034203.
(40) Macchia, E.; Manoli, K.; Holzer, B.; Di Franco, C.; Ghittorelli, M.; Torricelli, F.; Alberga, D.; Mangiatordi, G. F.; Palazzo, G.; Scamarcio, G.; Torsi, L. Single-Molecule Detection with a Millimetre-Sized Transistor. *Nat. Commun.* **2018**, *9* (1), 3223.
(41) Chaste, J.; Eichler, A.; Moser, J.; Ceballos, G.; Rurali, R.; Bachtold, A. A Nanomechanical Mass Sensor with Yoctogram Resolution. *Nat. Nanotechnol.* **2012**, *7* (5), 301.
(42) Park, S. J.; Kwon, O. S.; Lee, S. H.; Song, H. S.; Park, T. H.; Jang, J. Ultrasensitive Flexible Graphene Based Field-Effect Transistor (Fet)-Type Bioelectronic Nose. *Nano Lett.* **2012**, *12* (10), 5082−5090.
(43) Yu, W.; Jiang, W. C.; Lin, Q.; Lu, T. Cavity Optomechanical Spring Sensing of Single Molecules. *Nat. Commun.* **2016**, *7*, 12311.
(44) Naik, A. K.; Hanay, M.; Hiebert, W.; Feng, X.; Roukes, M. L. Towards Single-Molecule Nanomechanical Mass Spectrometry. *Nat. Nanotechnol.* **2009**, *4* (7), 445.
(45) Xia, M. A Review on Applications of Two-Dimensional Materials in Surface-Enhanced Raman Spectroscopy. *Int. J. Spectrosc.* **2018**, *2018*, 1.
(46) Levy, D.; Castellón, E. *Transparent Conductive Materials: Materials, Synthesis, Characterization, Applications*; John Wiley & Sons: 2018.
(47) Wang, X.; Shi, W.; She, G.; Mu, L.; Lee, S. High-Performance Surface-Enhanced Raman Scattering Sensors Based on Ag Nanoparticles-Coated Si Nanowire Arrays for Quantitative Detection of Pesticides. *Appl. Phys. Lett.* **2010**, *96* (5), 053104.
(48) Qiu, H.; Li, Z.; Gao, S.; Chen, P.; Zhang, C.; Jiang, S.; Xu, S.; Yang, C.; Li, H. Large-Area MoS_2 Thin Layers Directly Synthesized on Pyramid-Si Substrate for Surface-Enhanced Raman Scattering. *RSC Adv.* **2015**, *5* (102), 83899−83905.

DOI: 10.1021/acsanm.8b02308
ACS Appl. Nano Mater. 2019, 2, 1412−1420